Density and spatial distribution of charge carriers in the intrinsic *n*-type $LaAlO_3$-$SrTiO_3$ interface

Won-joon Son,[1] Eunae Cho,[1] Bora Lee,[1] Jaichan Lee,[2] and Seungwu Han[1,*]
[1]*Department of Physics, Ewha Womans University, Seoul 120-750, Korea*
[2]*School of Materials Science and Engineering, SungKyunKwan University, Suwon 440-746, Korea*
(Received 8 December 2008; revised manuscript received 8 May 2009; published 9 June 2009)

In order to establish the density and spatial distribution of charge carriers intrinsic to the *n*-type $LaAlO_3$-$SrTiO_3$ heterointerface, we carry out first-principles calculations on the $(LaAlO_3)_n(SrTiO_3)_{15}$ slab model with $n=2-10$. As the thickness of the $LaAlO_3$ layer increases, the charge transfer from $LaAlO_3$ to $SrTiO_3$ converges to half an electron per two-dimensional unit cell. It is found that the electrons in the conduction band of $SrTiO_3$ consist of various types of interface-bound states. The mobile electrons evaluated by excluding those states tightly bound to the interface within 2 nm or having large effective masses are in good agreement with the experimental carrier densities for all $LaAlO_3$ thicknesses, suggesting that the loosely bound states play a major role in the transport property. A large calculation including up to $(LaAlO_3)_5(SrTiO_3)_{30}$ shows that about 70% of electrons are confined within 3 nm from the interface, which is in good comparison with the experiments. It is found that the transferred electrons decay exponentially at short distances from the interface, but there is a crossover to an algebraically decaying region at ~4 nm.

DOI: 10.1103/PhysRevB.79.245411 PACS number(s): 73.20.−r, 73.40.−c, 71.15.−m

Since the seminal paper by Ohtomo and Hwang[1] reported the unexpected conductivity when two perovskite insulators, $SrTiO_3$ and $LaAlO_3$ (STO and LAO hereafter), form an atomically abrupt heterointerface along the [001] direction, much effort has been devoted to reveal its origin. Due to the alternating polarity of atomic layers in LAO along the [001] direction, the electrostatic potential diverges in LAO unless the electric charges are reconstructed at the interface. For stoichiometric interfaces, this results in a charge transfer between LAO and STO, which alters the electrostatic boundary condition such that the polar catastrophe is avoided.[2] However, it was demonstrated that oxygen vacancies can play a critical role depending on the oxygen pressure used in the growth or annealing stages.[3,4] Recently, it was also proposed that the cationic intermixing at the interface can result in the interfacial metallicity.[5]

While it has been repeatedly confirmed that the intrinsic *n*-type interface is conducting,[6,7] the carrier density and its spatial distribution are not fully understood. For example, the oxygen-annealed sample exhibits a saturated carrier density of $\sim 10^{13}$ cm^{-2} when the LAO is thicker than three unit cells.[3,7] This value is only a tenth of the nominal value expected from the electrostatic consideration, i.e., half an electron per two-dimensional unit cell or 3.2×10^{14} cm^{-2}.[2] Recently, based on the analysis of the Fermi surface and its impact on the correlation effects, Popović *et al.*[8] proposed that a significant portion of the charge carriers can be easily localized due to their strong two-dimensional nature or large effective masses. The density of mobile electrons contributed by loosely bound states was closer to the experimental measurements albeit still several times higher. On the other hand, the spatial extension of free carriers in STO was estimated to be tens of nanometers from the interface,[3] while the cross-sectional conducting-tip atomic force microscope (CT-AFM) revealed that it is as narrow as 7 nm.[9] A series of first-principles studies devoted to LAO-STO heterointerfaces[8,10–15] confirmed the metallic property of the *n*-type interface. However, the carrier density and its spatial distribution have not been highlighted much.[8,15] In addition, the thickness of STO was much smaller than the experimental scale, which limits the direct comparison with the experiment. In this paper, we perform the first-principles calculations with an aim of establishing the basic nature of electron carriers in the intrinsic LAO-STO interface. To minimize the artifact arising from the finite size of the model system, we employ large unit cells containing 15–30 layers of STO. The thickness of LAO is varied among one to ten layers to investigate how the carrier density is affected by the width of LAO. In addition, a vacuum layer is inserted to address the isolated property of the *n*-type interface.

The first-principles density functional calculations are performed using the VASP package.[16] The ion-electron interactions are described by the projector-augmented wave method,[17] and the local density approximation (LDA) is used to approximate the exchange-correlation energy of electrons.[18] The energy cutoff is chosen to be 400 eV, and the Brillouin zone was sampled on a $7\times 7\times 1$ regular mesh including the Γ point. The Gaussian smearing with a broadening width of 0.1 eV is used. A series of slab models of $(LAO)_n(STO)_{15}$ is calculated, which consists of *n* layers of LAO ($n=2$, 3, 4, 5, 6, 7, 9, and 10) and 15 layers of STO. The vacuum with a thickness of ~18 Å is inserted between neighboring slabs. The surface end of STO is terminated with one additional TiO_2 layer. It is found that if the surface is terminated with the SrO layer, the local conduction bottom is lower at the surface than inside the bulk, which affects the distribution of electron carriers. We consider only the *n*-type interface formed by a layer sequence of …-(SrO)-(TiO_2)-(LaO)-(AlO_2)-…. The two-dimensional lattice parameters are fixed to 3.87 Å, the theoretical cell parameter of bulk STO. This reflects the experimental condition that thin layers of LAO are grown on top of the STO substrate. Figure 1(a) shows the geometry of the simulation cell for $n=5$ $[(LAO)_5(STO)_{15}]$. The total length of the model

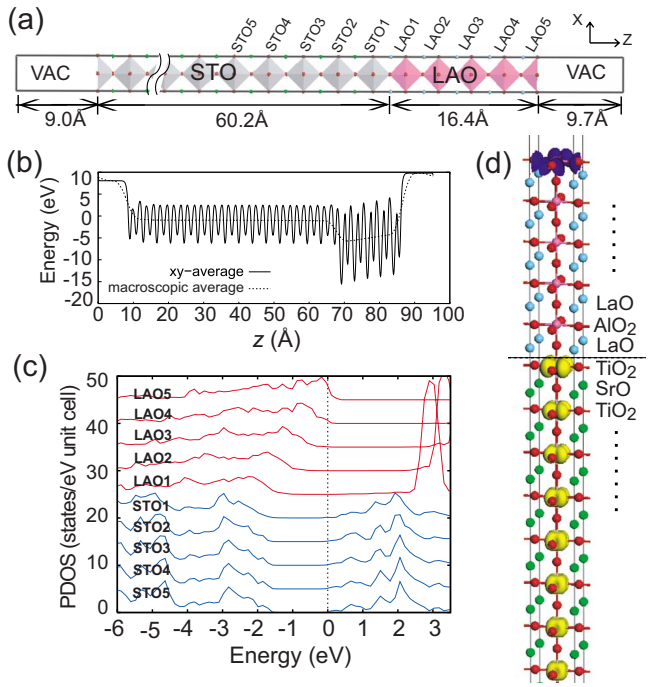

FIG. 1. (Color online) (a) The unit cell of $(LAO)_5(STO)_{15}$. (b) The *xy*-averaged (solid line) and macroscopically averaged (dashed line) local potential. Due to the artificial dipole moment introduced to screen the Coulomb potential from neighboring cells, there is a potential discontinuity in the middle of the vacuum region (z=0). (c) The partial density of states (PDOS) projected onto layers near the interface. The Fermi level is set to zero. (d) The spatial distributions of free electrons (light gray or yellow) and holes (dark gray or blue) in STO and LAO sides, respectively.

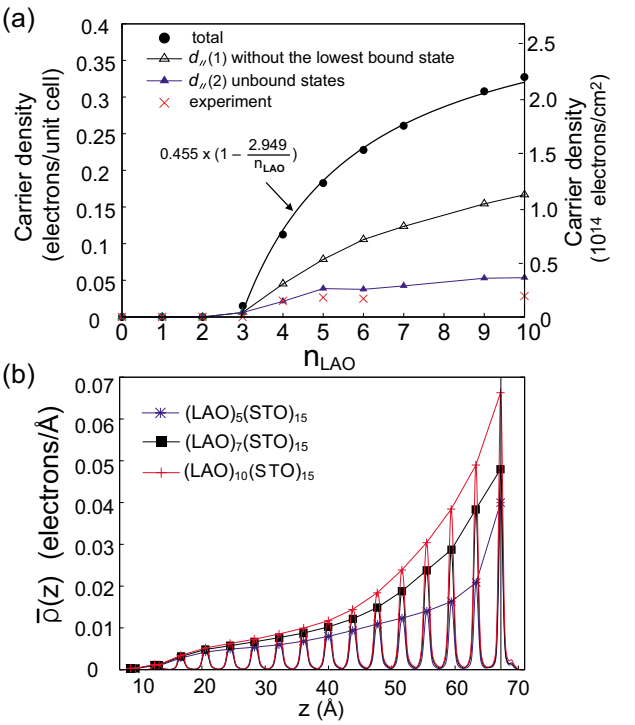

FIG. 2. (Color online) (a) Carrier densities of $(LAO)_n(STO)_{15}$ with respect to the number of LAO layers (n_{LAO}). The experimental data are presented as crosses (Ref. 1). The open and filled triangles indicate the contribution by $d_{\|}$ bands omitting the lowest subband alone [$d_{\|}(1)$] or several bands localized within ~2 nm from the interface [$d_{\|}(2)$], respectively. (b) The *xy*-averaged spatial distributions of transferred charges when n_{LAO} is 5, 7, and 10. The position of the interfacial Ti site is indicated by a vertical dashed line. For the visual purpose, the top position of each peak is linked with a line.

system including the vacuum region is ~9.5 nm for $(LAO)_5(STO)_{15}$. All atoms including surface layers are relaxed until atomic forces are reduced to within 0.02 eV/Å. A test calculation was also performed by fixing five layers from the STO surface, but the carrier density and spatial distribution were essentially the same as those in fully relaxed results. To remove the undesired electrostatic interaction between periodic cells along the z direction, the dipole correction as implemented in the code is applied.

Figures 1(b)–1(d) display electronic properties of $(LAO)_5(STO)_{15}$. The essential features are the same for all lengths of LAO. The *xy*-averaged (solid line) and macroscopically averaged[19] (dashed line) local potentials in Fig. 1(b) show that the potential increases in LAO due to the alternating polarity of atomic layers along the z direction with a slope of 0.13 V/Å. In Ref. 14, the corresponding slope was 0.24 V/Å for the five-layer LAO slab, which is higher than our value of 0.13 V/Å. (It is noted that for the three-layer slab, both works agree very well and the slope is ~0.2 V/Å.) This might be a consequence of the different methodology; while the LDA+U method was employed in Ref. 14, the present calculations are carried out within the conventional LDA framework. As a result, the band alignments between LAO and STO are dissimilar, which can significantly affect the charge transfer and the internal field inside LAO. The potential slope is ~0.2 V/Å for the three-layer slab where the charge transfer is close to zero (see below). From an electrostatic model assuming that one electron is transferred between LaO and AlO_2 unit cell, the dielectric constant of LAO is estimated to be ~30. This is in good comparison with a theoretical value of ~26 for rhombohedral LAO.[20]

In Fig. 1(c), the PDOS projected on interfacial layers of LAO or STO is displayed. It is found that the valence edge in LAO increases linearly in energy with the distance from the interface, which is in line with the potential increase in Fig. 1(b). This results in the hole creation at the top LAO layer (LAO5), as confirmed by the location of the Fermi level, and the electrons transfer from this layer to the conduction edges of STO. In Fig. 1(d), the spatial distribution of transferred electrons (light gray or yellow) and holes (dark gray or blue) is shown in STO and LAO sides, respectively. It can be observed that the holes are mostly O 2p orbitals in the top AlO_2 layer while the electrons are dominantly Ti 3d orbitals and spread over several STO layers. The lobe patterns at Ti sites indicate that the orbital character is d_{xy} at the interface, and it is gradually mixed with d_{xz} and d_{yz} at distant Ti sites from the interface.

By adding the occupation numbers of the states corresponding to the electrons transferred from LAO to STO, one can obtain the carrier density in STO. In Fig. 2(a), the carrier densities in STO are plotted as solid circles as a function of

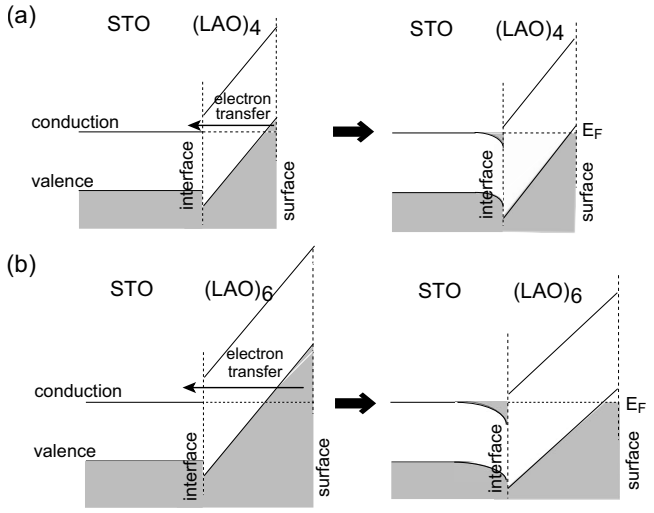

FIG. 3. Schematic diagrams to describe the carrier generation mechanism for two representative LAO thicknesses of (a) four and (b) six unit layers. The shaded parts are occupied by electrons. The left side of the figure shows the hypothetical situation where the charge transfer from LAO to STO is prohibited. The right side is the equilibrium state obtained in the self-consistent calculations with the well-defined Fermi level (E_F). Because of the charge transfer, the internal field inside LAO is smaller in the right sides.

the LAO thickness measured in unit cells (n_{LAO}). The critical thickness for a finite carrier density is found to be three layers, which is in good agreements with the experiment[7] and the previous theory.[12,14,21] (A small carrier density observed for $n_{\mathrm{LAO}}=3$ is in part due to the Fermi-level smearing.) However, it is noted that the energy gap of STO is 3.2 eV in experiment while the LDA underestimates it by ~1.5 eV. At the critical thickness, the valence top of LAO is in touch with the conduction bottom of STO (see below). Therefore, assuming that the valence-band offset at the interface is correctly described within LDA, the critical thickness should increase by around two layers when the true energy gap of STO is considered. Therefore, the agreement between the present LDA results and the experiment is rather surprising. However, there is a possibility that the true valence-band offset is significantly different from the LDA result such that the energy gap underestimation is effectively cancelled by the error in the valence-band offset. It is worth mentioning in this regard that the charge transfer is closely related to the total energy and electron density in the ground state, both of which are well described within LDA.

It is found in Fig. 2(a) that the carrier density increases with n_{LAO}. To explain this, we discuss the carrier generation mechanism in more detail. The electron transfer in the present model structure is a result of the increasing electrostatic potential inside the LAO slab which in turn originates from the alternating polarity of LaO and AlO_2 layers. To clarify this point, we present schematic diagrams in Fig. 3. The diagram shows spatially resolved band edges of STO and LAO with two different thicknesses [four and six unit layers for (a) and (b), respectively] that are larger than the critical value. The left side of the diagram depicts a hypothetical situation where the charge transfer from LAO to STO (Zener breakdown) is prohibited and therefore the system is in the nonequilibrium state. The internal field inside LAO is then maintained to that for the three-layer slab (~0.2 V/Å). When the thickness of LAO is larger than three unit cells, the local valence top of LAO in the surface region rises above the conduction bottom of STO, which triggers the electron transfer from LAO to STO. Even a small fraction of an electron transferred per unit area greatly lowers the internal electric field inside LAO because it is repeated two-dimensionally. Therefore, the iterative procedure leading to the self-consistency aligns the valence top of LAO in the surface region close to the conduction bottom of STO, resulting in the equilibrium state shown on the right side of Fig. 3. This means that the electric field inside LAO becomes smaller and smaller with the LAO thickness, which is a result of the larger charge transfer for thicker LAO slabs. Indeed, the internal field for $(\mathrm{LAO})_{10}(\mathrm{STO})_{15}$ is 0.07 V/Å in comparison with 0.13 V/Å for $(\mathrm{LAO})_5(\mathrm{STO})_{15}$ above. In the limit of $(\mathrm{LAO})_\infty$, the internal field should be zero, and this is precisely achieved by the charge transfer of half an electron.

Based on the schematic model in Fig. 3, one can derive a formula that connects the transferred electrons to the LAO thickness (d). Suppose that the average internal field within LAO is E_0 for the thickness smaller than the critical value, d_c. At $d=d_c$, the local valence top of LAO surface is in line with the conduction bottom of STO. This means that the energy gap (ΔE) from the valence top of LAO at the interface to the conduction bottom of STO is equal to eE_0d_c, where e is the electronic charge. For $d>d_c$, there is a finite charge transfer of $q(d)$ per unit supercell, which affects the internal field inside LAO [$E_{\mathrm{LAO}}(d)$] as follows:

$$E_{\mathrm{LAO}}(d) = E_0 - \frac{q(d)}{\varepsilon^0 A}, \tag{1}$$

where A is the unit area of the supercell along the xy plane and ε^0 is the static dielectric constant of LAO. It was explained above that the valence top of the surface LAO layer is closely aligned with the conduction bottom of STO for all LAO thicknesses. Therefore, one obtains the following relation as a first approximation:

$$\Delta E \simeq eE_{\mathrm{LAO}}(d)d = e\left(E_0 - \frac{q(d)}{\varepsilon^0 A}\right)d. \tag{2}$$

Since $\Delta E=eE_0d_c$,

$$\left(E_0 - \frac{q(d)}{\varepsilon^0 A}\right)d = E_0 d_c. \tag{3}$$

Rearranging Eq. (3) leads to the following formula for the charge transfer:

$$q(d) = \varepsilon^0 A E_0\left(1 - \frac{d_c}{d}\right). \tag{4}$$

Since the electric field in (LaO)-(AlO_2) is $e/\varepsilon^0 A$ while that in (AlO_2)-(LaO) is zero, the average internal field is $E_0 = 0.5e/\varepsilon^0 A$. Therefore,

$$q(d) = 0.5e\left(1 - \frac{d_c}{d}\right). \quad (5)$$

Equation (5) shows that the charge transfer is dictated solely by the critical thickness and does not depend on the electronic properties of LAO such as the dielectric constant. For the semi-infinite LAO ($d=\infty$), half an electron is transferred per unit supercell, which is consistent with the condition to avoid the polar catastrophe. We fit the functional form in Eq. (5) to the data in Fig. 2(a) with the prefactor as an additional variational parameter and obtain $q(n_{\mathrm{LAO}}) = 0.455e(1-2.949/n_{\mathrm{LAO}})$. The prefactor 0.455 is close to the ideal value of 0.5, and the critical thickness of three layers is also in good agreement with data in Fig. 2(a).

In reality, a range of imperfections can be introduced during the experimental growth. Among them, certain defects, notably the oxygen vacancy, can themselves induce a charge transfer from the surface to the interface. If repeated over the surface, such a charge-transfer defect can flatten the internal field of LAO and consequently weaken the dependence of the carrier density on the LAO thickness. Moreover, the electrostatic instability built upon the internal field of LAO could reduce the formation energy of the charge-transfer defects. For instance, in the supplementary information of Ref. 19, it was shown that the oxygen vacancy repeated over the LAO surface with 2×2 periodicity lowers the surface free energy for a certain range of the oxygen chemical potential (and results in the flat band inside LAO). However, it should be noted that the *n*-type interface is insulating in experiment for the LAO thickness less than four layers, which is exactly reproduced in the present work based on the clean surface. This implies that the density of charge-transfer defects is not significant at least for thin LAO layers because any such defects should render the interface conducting. However, one cannot rule out the possibility that the charge-transfer defects such as oxygen vacancies become important for thicker LAO films.

The experimental free carrier densities[7] are marked as crosses in Fig. 2(a). Notably, the magnitude of the carrier density is smaller than the theoretical predictions by an order. In addition, discrepancies are also observed in the thickness dependence, and the experimental carrier density does not change meaningfully when n_{LAO} is larger than the critical value. In Fig. 2(b), the *xy*-averaged distribution of the transferred electrons $[\bar{\rho}(z)]$ is shown for various thicknesses of LAO. It is noticeable that the density rises faster in the interface region than in the tail part near the STO surface. This is due to a strong attractive potential near the interface that is exerted by the positive holes at the LAO surface.

Figure 4(a) shows the band structure of the $(\mathrm{LAO})_5(\mathrm{STO})_{15}$ along the special points in the surface Brillouin zone. The parabolic bands above the Fermi level are derived from the conduction bands of STO, split by the finite size of STO and the attractive potential at the interface. The positive holes at the LAO surface can be identified at the *M* point (dashed circle) while the free carriers in STO are at the Γ point (solid circle) and should consist of t_{2g} level at Ti sites. The threefold degeneracy of the t_{2g} level is lifted by the presence of the interface, and the t_{2g} manifold is divided into

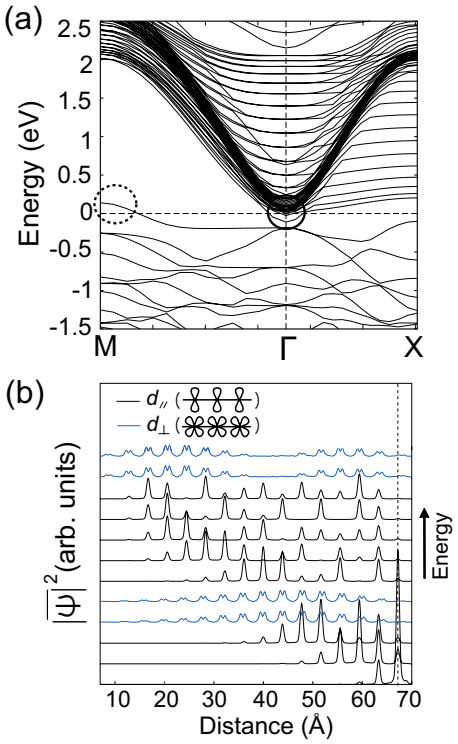

FIG. 4. (Color online) (a) Band structure of $(\mathrm{LAO})_5(\mathrm{STO})_{15}$ along the special points in the surface Brillouin zone. The Fermi level is set to zero. (b) *xy* average of squared wave functions for low-lying energy states in the solid circle of (a). $d_{\parallel}$ and $d_{\perp}$ mean that the plane of Ti 3*d* orbital is parallel and perpendicular to the interface plane, respectively. The vertical dashed line shows the position of interfacial Ti site. The figures in the legend are schematic geometries of Ti 3*d* orbitals along the interface normal.

d_{xy} ($d_{\parallel}$; parallel to the interface) and $d_{xz(yz)}$ ($d_{\perp}$; perpendicular to the interface).

The band structure in Fig. 4(a) is largely similar to that in Ref. 8; the lowest band near the Γ point is composed of $d_{\parallel}$ orbitals localized at the interfacial Ti site, and $d_{\perp}$ subbands show small dispersions from Γ to *X* points. However, there are two places that the two band structures do not agree on quantitatively. First, the relative Fermi-level position from the bottom of the lowest $d_{\parallel}$ band is much higher in Ref. 8, meaning that the carrier density is larger in that work. This discrepancy stems from the disparate model structures. In Ref. 8 (and also in Ref. 10, 11, and 13), a symmetric model interface was employed without the vacuum layer. This results in the nonstoichiometric LAO slab with one additional LaO layer. This extra layer gives out an electron per unit area which goes to the conduction bottom of STO. Since there are two interfaces within the model, each interface equally accommodates half an electron. In this type of model structure, the amount of the electron transfer does not depend on the LAO thickness, in contrast to the results based on the stoichiometric LAO and STO slabs as in the present work (and also in Refs. 12 and 14). As described above, the carrier generation in this work is a consequence of the internal field of LAO and the electron transfer is much smaller than half an electron when the thickness of LAO is five layers. Therefore, the Fermi-level position is closer to the bottom of $d_{\parallel}$

bands compared to that in Ref. 8. This is also related to another discrepancy in the band structure, that is to say, the energy difference between the lowest two $d_{\|}$ bands at the Γ point. In Ref. 8, the value is 0.3 eV while our value is only 0.1 eV. This is because the stronger interfacial potential in that work, which was caused by the larger charge transfer, tends to stabilize localized states preferentially. Indeed, as the thickness of LAO increases, the energy gap between the lowest two $d_{\|}$ bands increases also in our calculations. [For instance, the corresponding value for the $(LAO)_{10}(STO)_{15}$ structure is 0.2 eV.]

The band structure in Fig. 4(a) also indicates the existence of hole states in the surface layer. An intriguing question is whether this means the surface conductivity of LAO. We are not aware of any experiment reporting the conducting surface of LAO. However, it is noted that the hole states are mostly O $2p$ orbitals in the surface AlO_2 layer as shown in Fig. 1(d). Based on an argument similar to that applied to the interface-localized Ti $3d$ orbitals in Ref. 8 (also see below), the surface hole state would be easily localized in the presence of impurities and/or surface roughness. In addition, it was shown in Ref. 10 that the correlated band theory applied to the O $2p$ orbitals can result in the localized polaron in the interfacial AlO_2 layer, which was proposed as a possible explanation on the insulating nature of p-type interface. The same thing may happen to the surface hole states as well because orbital characters are very similar. To add, in many transport measurements of LAO-STO interface, some (nonpolar) insulating materials (such as amorphous LAO) are deposited on top of the epitaxial LAO layer. In this case, the interface between LAO and the insulating overlayer is ill defined and the positive hole would be created in the form of fixed charges rather than extended interface states. Such fixed charges may affect the carrier mobility and dependence on gate voltages but will not be detected as conducting carriers.

In Fig. 4(a), several states cross the Fermi level near the Γ point, which means that the charge carrier consists of many different bands. In order to identify electronic characters, we further analyze those states at the Γ point with appreciable occupation numbers [a solid circle in Fig. 3(a)]. Figure 3(b) shows the xy average of squared wave functions $[\overline{|\psi|^2}(z)]$ in the order of energy (the bottom state is the lowest in energy). The peak positions coincide with Ti sites in TiO_2 layers. It is seen that the electronic states are quantized at the interface with increasing localization widths for higher states, which is similar to the Airy functions in a wedge potential. It is notable that $\overline{|\psi|^2}$ is singly or doubly peaked at Ti sites. Each of them corresponds to $d_{\|}$ and $d_{\perp}$, respectively, implying that the threefold degeneracy of t_{2g} level is lifted, as discussed above. In Fig. 3(b), several low-lying $d_{\|}$ states are tightly bound at the interface. In particular, the lowest state shows the maximum intensity at the interfacial Ti layer (vertical dashed line). In contrast, doubly degenerate lowest $d_{\perp}$ states have a node at the interface boundary. This can be understood on the basis of the orbital geometry; the spatial distribution of $d_{\perp}$ orbitals is more extended along the interface normal than for $d_{\|}$ orbitals [see legends in Fig. 3(b)]. Therefore, $d_{\perp}$-derived states would be more sensitive to the band discontinuity at the interface. That is to say, that $d_{\perp}$ states are effectively subjected to an infinite barrier at the interface. It is also noticeable in Fig. 3(b) that the envelope profile of $d_{\perp}$ states is more delocalized compared to $d_{\|}$ states. This can be explained in terms of the effective mass of each band; in $d_{\perp}$ states, $d_{xz(yz)}$ orbitals along the surface normal overlap with each other mediated by O $2p$ orbitals while $d_{\|}$ bands are rather disconnected in the same direction. Therefore the effective mass along the surface normal should be bigger for $d_{\|}$ bands, which results in tighter distributions of $d_{\|}$ bands.

In Ref. 8, it was suggested that the lowest $d_{\|}$ subband might be easily localized due to its strong two-dimensional character. In addition, $d_{\perp}$ bands were also assumed to be localized because of heavy effective masses along the interface direction. Following this idea, we evaluate the mobile carrier density that contributes to the actual conductivity. In Fig. 2(a), the open triangles indicate the active carrier densities obtained in this way. They are much lower than the total carrier density but still several times bigger than the experimental values. (A similar observation was reported in Ref. 8.) We then try to omit $d_{\|}$ bands that are localized within ~2 nm from the interface because these states would be easily scattered by the interface roughness which is about 1 nm.[2] For example, this means that three low-lying states in Fig. 4(b) are excluded in the case of $(LAO)_5(STO)_{15}$. The data are shown as filled triangles in Fig. 2(a). It is found that the magnitude of the effective carrier density is similar to the experimental measurements and the saturation behavior is also observed. The slow increase in the carrier density originates from the fact that the interface potential becomes deeper with the LAO thickness and the occupation numbers for the interface-bound states increase much faster than for the loosely bound states. The agreement with the experiment could be accidental since there is no clear-cut boundary to decide whether a specific state is prone to localization or scattering. However, these results strongly indicate that the loosely bound states play a major role in the transport measurement, as was suggested in Ref. 8.

Finally, to investigate the spatial extension of the transferred electrons in STO, we increase the number of STO unit layers up to 30 while the number of LAO unit layers is fixed to five. The total length of STO is then as much as 12 nm. In Fig. 5, the distributions of transferred electrons $[\bar{\rho}(z)]$ are compared among $(LAO)_5(STO)_{10}$, $(LAO)_5(STO)_{15}$, $(LAO)_5(STO)_{20}$, and $(LAO)_5(STO)_{30}$. The charge densities are aligned at the interface position. It is observed that the carrier distribution at the interface does not change much while a small amount of charges in the tail part is extended to the surface of the STO slab even for $(LAO)_5(STO)_{30}$. Consistently, the occupation numbers corresponding to the lowest-energy band does not change appreciably for all lengths of STO.

In Table I, we summarize the total transferred electrons and its fraction within 3 nm from the interface. It is found that good convergences are achieved with $(LAO)_5(STO)_{30}$ and about 70% of total transferred charges are confined within 3 nm from the interface. This is in good comparison with the electron-energy-loss spectroscopy (EELS) (Ref. 2) and CT-AFM image[9] on the annealed LAO-STO interface. We note that the EELS detects the chemical states of Ti so it would reflect the distribution of whole charges (not just mo-

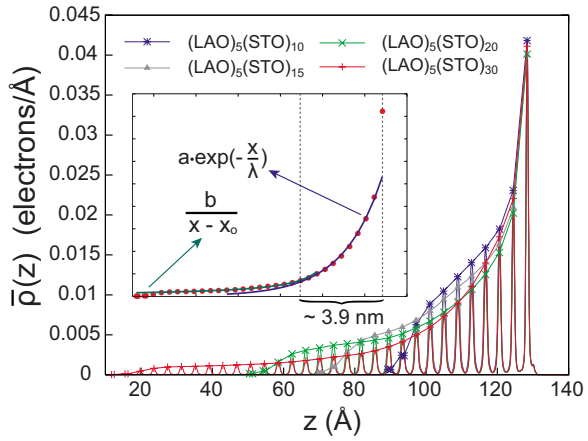

FIG. 5. (Color online) Spatial distributions of *xy*-averaged carriers with various thicknesses of STO. The figures are aligned at the interfacial Ti site (dashed line). As a visual guide, the top position of each peak is connected with a line. In the inset, the charge distribution for $(LAO)_5(STO)_{30}$ is fitted with two functional forms with respect to the distance x from the interfacial TiO_2 layer. Fitted values are $a=0.027$ electrons/Å, $\lambda=18.35$ Å, $b=0.082$ electrons, and $x_0=15.90$ Å

bile carriers). On the other hand, CT-AFM measures the conductivity along the interface, and therefore it might be related to the mobile carriers. In this case, some of interface-bound states should be excluded for a fair comparison of the spatial distribution, as was done in evaluating the active carriers in Fig. 2(a), and this would yield a broader charge distribution.

Our result is at variance with Ref. 3 in which the spatial extension of the intrinsic carrier was estimated to be as much as tens of nanometers at 4 K. This was attributed to a large dielectric constant of STO (~20 000) at low temperatures. At 300 K, the dielectric constant of bulk STO is around 300 and the same macroscopic model predicted a much narrower distribution, underscoring the importance of the dielectric constant to the distribution of the charge carrier. Because of two interfacial effects, it is likely that the dielectric constant of STO is significantly suppressed near the interface; first, a high tunability of STO indicates that the strong electric field at the interface (up to ~1 V/nm) can lower the dielectric constant significantly.[22] Second, it was shown that the intrinsic dead layer with low dielectric constants exist at the metal-STO interface.[23–25] A similar effect is likely to occur at the LAO-STO interface. As was shown above, about 70% of electrons are confined within 3 nm from the interface, where the interfacial effects might be strong. Therefore, the primary distribution of the transferred electrons would be well captured in the present work even though LDA calculations underestimate the dielectric constant of bulk STO significantly (at low temperatures). However, the decay length in the tail part might be underestimated in this work because the dielectric constant of bulk STO becomes relevant in this region.

TABLE I. Total charge transfer and its fraction within 3 nm from the interface for various thicknesses of STO.

Model	Total charge transfer (e)	Charge fraction within 3 nm from the interface (%)
$(LAO)_5(STO)_{10}$	0.176	91.1
$(LAO)_5(STO)_{15}$	0.183	71.9
$(LAO)_5(STO)_{20}$	0.181	67.3
$(LAO)_5(STO)_{30}$	0.183	71.3

In Ref. 15, the exponential decay of the charge density was found and it was attributed to the quantum mechanical effects related to the metal-induced gap states. Motivated by this work, we try to fit the charge distribution for $(LAO)_5(STO)_{30}$ with an exponential function in the form of $a\times\exp(-x/\lambda)$, where x is the distance from the interfacial TiO_2 layer. However, we were not able to fit the whole data with a single exponent. As shown in the inset of Fig. 5, except for the data for the first TiO_2 layer, the region close to the interface was reasonably fitted with an exponentially decaying form with the attenuation length of 18.35 Å. However, for $x>4$ nm the charge density decays much slowly and the data are fitted better to an algebraic function, for example, in the form of $b/(x\text{-}x_0)$. As shown in Fig. 4(b), the low-lying states comprising the carrier density show the energy-dependent confinement due to the wedgelike potential generated by the positive hole at the LAO surface. The exponential decay is an average effect of this. Since the wedge potential is screened by transferred charges, the electrons further from the interface feel progressively weaker potential, resulting in the slowly decaying distribution. Therefore, our analysis seems to be at variance with the conclusion in Ref. 15. In addition, the careful analysis of PDOS in Fig. 1(c) indicates that the energy gap of bulk STO is recovered from the third STO layer, in contrast with Ref. 15 where the energy gap is significantly reduced even for the farthest layer from the interface.

In summary, we carried out first-principles calculations on the *n*-type LAO-STO interface by varying the thickness of both LAO and STO. It was found that the charge transfer from LAO to STO increases with the thickness of LAO. Even though the total sum of charge carriers was much larger than the experimental observations, the contribution by loosely bound states showed much better agreement, suggesting that these states may play a unique role in the transport property of the *n*-type interface as has been suggested in a recent paper.[8] A large calculation with the STO length increased up to 12 nm showed that about 70% of transferred electrons are confined within ~3 nm from the interface, in good comparison with experimental images. The transferred electrons decay exponentially at short distances from the interface, but there is a crossover to an algebraically decaying region at ~4 nm

We thank Dong-Wook Kim and Jaejun Yu for helpful discussions. This work was supported by the Korea Research Foundation Grant funded by the Korean Government (MOEHRD) (Grant No. KRF-2007-314-C00080) and the KOSEF through the National Research Laboratory (NRL) program and Quantum Metamaterials Research Center (Grant No. R11-2008-053-03001-0).

*Corresponding author; hansw@ewha.ac.kr

[1] A. Ohtomo and H. Y. Hwang, Nature (London) **427**, 423 (2004).
[2] N. Nakagawa, H. Y. Hwang, and D. A. Muller, Nature Mater. **5**, 204 (2006).
[3] W. Siemons, G. Koster, H. Yamamoto, W. A. Harrison, G. Lucovsky, T. H. Geballe, D. H. A. Blank, and M. R. Beasley, Phys. Rev. Lett. **98**, 196802 (2007).
[4] A. Kalabukhov, R. Gunnarsson, J. Börjesson, E. Olsson, T. Claeson, and D. Winkler, Phys. Rev. B **75**, 121404(R) (2007).
[5] P. R. Willmott, S. A. Pauli, R. Herger, C. M. Schlepütz, D. Martoccia, B. D. Patterson, B. Delley, R. Clarke, D. Kumah, C. Cionca, and Y. Yacoby, Phys. Rev. Lett. **99**, 155502 (2007).
[6] M. Huijben, G. Rijnders, D. H. A. Blank, S. Bals, S. V. Aert, J. Verbeeck, G. V. Tendeloo, A. Brinkman, and H. Hilgenkamp, Nature Mater. **5**, 556 (2006).
[7] S. Thiel, G. Hammerl, A. Schmehl, C. W. Schneider, and J. Mannhart, Science **313**, 1942 (2006).
[8] Z. S. Popović, S. Satpathy, and R. M. Martin, Phys. Rev. Lett. **101**, 256801 (2008).
[9] M. Basletic, J.-L. Maurice, C. Carrétéro, G. Herranz, O. Copie, M. Bibes, É. Jacquet, K. Bouzehouane, S. Fusil, and A. Barthélémy, Nature Mater. **7**, 621 (2008).
[10] R. Pentcheva and W. E. Pickett, Phys. Rev. B **74**, 035112 (2006).
[11] J.-M. Albina, M. Mrovec, B. Meyer, and C. Elsässer, Phys. Rev. B **76**, 165103 (2007).
[12] S. Ishibashi and K. Terakura, J. Phys. Soc. Jpn. **77**, 104706 (2008).
[13] M. S. Park, S. H. Rhim, and A. J. Freeman, Phys. Rev. B **74**, 205416 (2006).
[14] J. Lee and A. A. Demkov, Phys. Rev. B **78**, 193104 (2008).
[15] K. Janicka, J. P. Velev, and E. Y. Tsymbal, Phys. Rev. Lett. **102**, 106803 (2009).
[16] G. Kresse and J. Hafner, Phys. Rev. B **47**, 558 (1993).
[17] P. E. Blöchl, Phys. Rev. B **50**, 17953 (1994).
[18] D. M. Ceperley and B. J. Alder, Phys. Rev. Lett. **45**, 566 (1980).
[19] A. Balderschi, S. Baroni, and R. Resta, Phys. Rev. Lett. **61**, 734 (1988).
[20] S. A. Shevlin, A. Curioni, and W. Andreoni, Phys. Rev. Lett. **94**, 146401 (2005).
[21] C. Cen, S. Thiel, G. Hammerl, C. W. Schneider, K. E. Andersen, C. S. Hellberg, J. Mannhart, and J. Levy, Nature Mater. **7**, 298 (2008).
[22] A. Antons, J. B. Neaton, K. M. Rabe, and D. Vanderbilt, Phys. Rev. B **71**, 024102 (2005).
[23] M. Stengel and N. A. Spaldin, Nature (London) **443**, 679 (2006).
[24] B. Lee, C.-K. Lee, J. Lee, C. S. Hwang, and S. Han, J. Appl. Phys. **103**, 024106 (2008).
[25] B. Lee, S. Han, and J. Lee, J. Korean Phys. Soc. **52**, 70 (2008).